(Preprint) IAA-AAS-SciTech-039

NEAR RECTILINEAR HALO ORBITS IN CISLUNAR SPACE WITHIN THE CONTEXT OF THE BICIRCULAR FOUR-BODY PROBLEM

Kenza Boudad[*], Kathleen Howell[†], Diane Davis[‡]

As evidenced by the Global Exploration Roadmap, international interest exists in a new era of human exploration of the solar system. Such an effort is commencing with the examination of options for maintaining a facility – at times crewed – in an orbit nearby the Moon. Thus, the key objectives in advancing colonization of interplanetary space include positioning and maintaining an inhabited facility in a long-term and relatively stable orbit in the lunar vicinity. At this time, one orbit of interest for a habitat spacecraft in cislunar space is a Near Rectilinear Halo Orbit (NRHO). Near Rectilinear Halo Orbits are members of the L_1 or L_2 halo orbit families and are characterized by favorable stability properties. As such, they are strong candidates for a future habitat facility in cislunar space. This type of trajectory was first identified in cislunar space—the Earth-Moon CR3BP. However, for arrival to and departure from this Earth-Moon region, the impact of Solar gravity cannot be ignored. Thus, the orbital characteristics and stability properties are examined within the context of the bicircular restricted four-body problem.

INTRODUCTION

The proposed Gateway concept is the current framework for the NASA development of a space facility near the Moon with an option to return to the lunar surface.[1–3] From a baseline trajectory in a Near Rectilinear Halo Orbit (NRHO), the Gateway is intended to serve as a proving ground for deep space technologies and as a staging location for missions beyond cislunar space. The NRHOs are members of the L_1 or L_2 families as defined within the context of the Circular Restricted Three-Body Problem (CR3BP), representing the Earth-Moon system. As such, they are characterized by favorable stability characteristics.

The NRHOs are defined within the context of the CR3BP. However, for arrival and departure from the Earth-Moon region, the impact of the solar gravity is significant. The Sun and its location in the Earth-Moon frame is also relevant when exploring the orbits for characteristics that translate to the higher-fidelity ephemeris model. The perturbing effects of the Sun on the orbit as it expands out from the lunar vicinity are crucial to any baseline trajectory. Thus, in this investigation, the gravitational impact is assessed in the Bicircular Restricted Four-Body Problem (BCR4BP) that incorporates solar gravity, reasonably represents the full range of epoch dates and supports eventual transition to an ephemeris model. To successfully construct trajectories in this regime, the ability to translate the characteristics to higher-fidelity models is critical. This examination of a baseline trajectory in the BCR4BP adds insight in the design process.

[*]Ph.D. Student, School of Aeronautics and Astronautics, Purdue University, West Lafayette, IN 47907; kboudad@purdue.edu

[†]Hsu Lo Distinguished Professor of Aeronautics and Astronautics, School of Aeronautics and Astronautics, Purdue University, West Lafayette, IN 47907; howell@purdue.edu

[‡]Principal Systems Engineer, a.i.solutions, Inc., 2224 Bay Area Blvd, Houston TX 77058; diane.davis@ai-solutions.com

DYNAMICAL MODELS

Two dynamical models are employed in this investigation. The Circular Restricted Three-Body Problem (CR3BP) is an autonomous model approximating the Earth-Moon system dynamics. The Bicircular Restricted Four-Body Problem (BCR4BP) is a time-dependent, periodic model describing the motion of a particle in the Earth-Moon-Sun regime. The BCR4BP is an intermediate step between the CR3BP and a high-fidelity, time-dependent, non-periodic ephemeris model.

The Circular Restricted Three-Body Problem

In the CR3BP, the motion of a centrobaric, massless spacecraft is subject to the influence of two primary gravitational bodies, for example, the Earth and the Moon. The model assumes that the two primaries are point masses moving about their common center of mass in circular orbits. The motion of the spacecraft under the influence of the two primaries is described relative to a rotating frame at a fixed rate consistent with the rotation of the primaries. By convention, the differential equations governing the CR3BP are nondimensionalized. The characteristic quantities employed include: (i) the Earth-Moon distance; (iii) the sum of the primary masses; (iii) a characteristic time such that the nondimensional gravitational constant $\tilde{G}$ equals unity. The nondimensional equations of motion are then

$$\ddot{x} \;\; = 2\dot{y} + \tfrac{\partial U^*}{\partial x}, \quad \ddot{y} \;\; = -2\dot{x} + \tfrac{\partial U^*}{\partial y}, \quad \ddot{z} \;\; = \tfrac{\partial U^*}{\partial z} \tag{1}$$

where x, y, z (respectively, $\dot{x}, \dot{y}, \dot{z}$) are the nondimensional position (respectively, the velocity) components of the spacecraft relative to the barycenter and expressed in terms of the Earth-Moon rotating frame. The pseudo-potential U^* is defined as

$$U^* = \frac{1}{2}(x^2 + y^2) + \frac{\mu}{r_{\text{e-sc}}} + \frac{1-\mu}{r_{\text{m-sc}}} \tag{2}$$

The quantities $r_{\text{e-sc}}$ and $r_{\text{e-sc}}$ are the distances between the spacecraft and the primaries, and $\mu = {}^{m_{\text{m}}}\!/_{m_{\text{e}}+m_{\text{m}}}$ is the mass parameter for the Earth-Moon CR3BP system.

The equations of motion in the CR3BP do not admit a closed form solution. However, five equilibrium points, or libration points, exist and are denoted L_1 through L_5. Stable and unstable planar and three-dimensional orbit families also exist in the CR3BP: the planar Lyapunov and the three-dimensional halo families, in particular, are associated with the libration points. A single integral of the motion, i.e., the Jacobi constant, exists in the CR3BP and is evaluated as

$$C = 2U^* - \left(\dot{x}^2 + \dot{y}^2 + \dot{z}^2\right) \tag{3}$$

The Jacobi constant is an energy-like quantity and serves to bound the motion.

The Bicircular Restricted Four-Body Problem

In scenarios where the gravitational influence of the Sun is non-negligible, a higher-fidelity model is necessary to accurately describe the spacecraft behavior. The BCR4BP incorporates the gravitational effect of three massive bodies, for instance, the Earth, the Moon and the Sun, on the motion of a spacecraft.[4] The mass of the spacecraft is assumed to be negligible in comparison to the masses of the other bodies. In this model, the Earth and the Moon are assumed to move in circular orbits around their common barycenter, denoted B_1, while the Sun and B_1 move in circular orbits with respect to the Earth-Moon-Sun barycenter, labeled B_2, as denoted in Figure 1. The BCR4BP is not a coherent model: the perturbing acceleration from the Sun does not influence the motion of the Earth

and the Moon, thus, the motion of the Moon is not a solution to the Sun-Earth CR3BP. Coherent bicircular models have been investigated previously,[5] but are not necessary in this analysis. The equations of the motion in the CR3BP in Equation (1) are extended to include the solar gravitational influence as follows,

$$\ddot{x} = 2\dot{y} + \frac{\partial \Upsilon^*}{\partial x}, \quad \ddot{y} = -2\dot{x} + \frac{\partial \Upsilon^*}{\partial y}, \quad \ddot{z} = \frac{\partial \Upsilon^*}{\partial z} \tag{4}$$

where Υ^* is the pseudo-potential function in the BCR4BP

$$\Upsilon^* = U^* + \frac{m}{r_{\text{s-sc}}} - \frac{m}{a^3}(x_{\text{s}}x + y_{\text{s}}y + z_{\text{s}}z) \tag{5}$$

and $m = \frac{m_{\text{s}}}{m_{\text{e}}+m_{\text{m}}}$ is the nondimensional mass of the Sun, and $a = \frac{r_{\text{s}}}{r_{\text{e-m}}}$ is the nondimensional distance between the Earth-Moon barycenter and the Sun. Then, $x_{\text{s}}, y_{\text{s}}, z_{\text{s}}$ are the position components of the Sun, originating at B_1, and expressed in terms of the Earth-Moon rotating frame,

$$\begin{bmatrix} x_{\text{s}} \\ y_{\text{s}} \\ z_{\text{s}} \end{bmatrix} = a \begin{bmatrix} \cos(\theta_{\text{s}}) \\ \sin(\theta_{\text{s}}) \\ 0 \end{bmatrix} \begin{bmatrix} \cos(\omega_{\text{s}}\, t + \theta_{\text{s0}}) \\ \sin(\omega_{\text{s}}\, t + \theta_{\text{s0}}) \\ 0 \end{bmatrix} \tag{6}$$

where $\omega_{\text{s}} = -0.9253$ is the nondimensional angular velocity of the Sun as viewed in the Earth-Moon rotating frame and the Sun angle θ_S is measured from the rotating $\hat{x}$ axis to the Sun position vector. Observe that the independent time variable, t, explicitly appears in the BCR4BP pseudo-

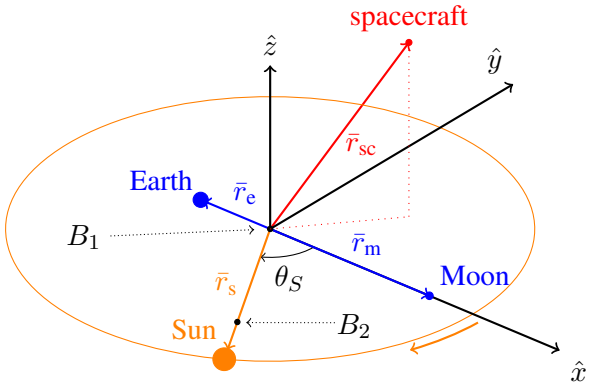

Figure 1: **BCR4BP in the Earth-Moon rotating frame**

potential. Therefore, the BCR4BP is time-dependent and does not admit an integral of the motion. However, a scaled version of the Hamiltonian is defined to be consistent with the Jacobi constant in the CR3BP, i.e.,

$$H(\theta_{\text{s}}) = 2\Upsilon^* - \left(\dot{x}^2 + \dot{y}^2 + \dot{z}^2\right) \tag{7}$$

The time-dependent nature of the differential equations in the BCR4BP yields time-dependent equilibrium solutions. These instantaneous equilibrium solutions correspond to the perturbed, or oscillating, CR3BP libration points (L_i), and are denoted $E_1(\theta_{\text{s}})$ through $E_5(\theta_{\text{s}})$. Note that the relative positions of the primaries in the BCR4BP are periodic: one period corresponds to the time between two alignments of the Earth, the Moon and the Sun (in this order) and is approximately equal to 29.5 days, i.e., one synodic period. The angular rate associated with the Earth-Moon rotating frame corresponds to the *sidereal* period of the system, that is, approximately 27.2 days, whereas the orbits of interest in this investigation are related to the system's *synodic* period.

NEAR RECTILINEAR HALO ORBITS

The halo family and its subset, the Near Rectilinear Halo Orbits (NRHOs), are three-dimensional periodic orbits as defined in the CR3BP. The halo family bifurcates from each family of planar Lyapunov orbits associated with the collinear libration points. For the L_1 and the L_2 equilibrium points in the Earth-Moon system, the halo family originates in the x-y plane from the bifurcation orbit in the Lyapunov family, and evolves out of plane as the family of orbits approaches the Moon. Note that the halo family is mirrored across the x-y plane: the northern family members possess a positive z component over the majority of their orbit, while the southern family members are defined by a negative z component. The NRHO subset of the L_1 and L_2 halo families are delineated by their linear stability properties.[6] Representative southern L_1 and L_2 halo orbits in the Earth-Moon system appear in Figure 2.

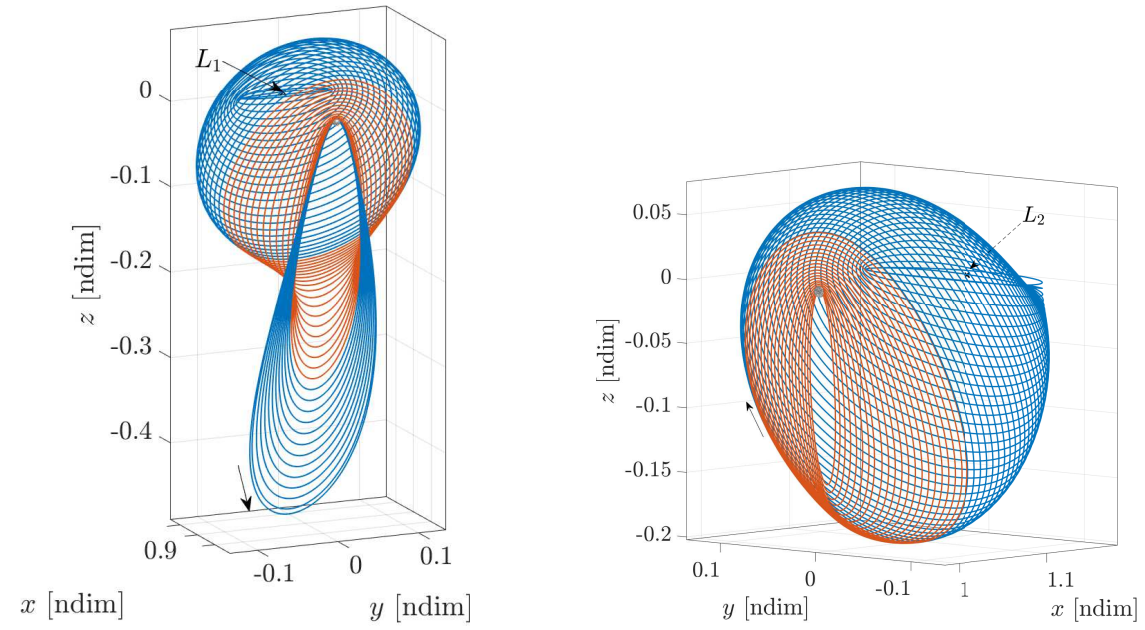

Figure 2: **3D view of the CR3BP Earth-Moon L_1 (a) and L_2 halo families. Members of the NRHO subset are colored in orange.**

Periodic orbits in the BCR4BP

Periodic orbits in the CR3BP are solutions that precisely repeat in all six position and velocity states (x, y, z, $\dot{x}$, $\dot{y}$ and $\dot{z}$) over every period. Previous contributions demonstrate that an infinity of periodic orbits exist in the CR3BP.[7,8] Various numerical approaches to construct CR3BP periodic solutions include linearizing the equations of motion in the vicinity of the equilibrium points and leveraging the symmetry properties in the system with the mirror theorem[9] and a targeting scheme.

The BCR4BP is formulated to represent a time-dependent, periodic system. Therefore, only isolated periodic orbits with specific periods exist rather than families with continuously varying periods.[10] While CR3BP periodic solutions only require periodicity in 6 states, periodic solutions

in the BCR4BP require an additional condition, i.e., the Sun location must also be commensurate with the periodic cycle over which the states repeat. Thus, the period for any periodic orbit in the BCR4BP is a multiple of the Earth-Moon-Sun period, that is, approximately 29.5 days. Thus, all periodic solutions in the BCR4BP are isolated synodic periodic solutions.

Initial guess generation

Initial guess generation for periodic solutions in the BCR4BP is achieved by leveraging the synodic resonant orbits in the CR3BP. Synodic resonant orbits are characterized by an integer ratio between the lunar synodic period and the orbital period. This ratio is represented as N:Q, where N is the number of orbital periods and Q is equal to the number of lunar synodic periods. Plotting the ratio across a family against another parameter, such as the perilune radius, uncovers the resonant family members. Resonance plots for the L_1 and the L_2 Earth-Moon CR3BP halo families appear in Figure 3. Members of the NRHO subset along the halo family are colored in orange. Note that the evolution of the period is not monotonic for the L_1 family, in Figure 3(a). Thus, multiple orbits with the same

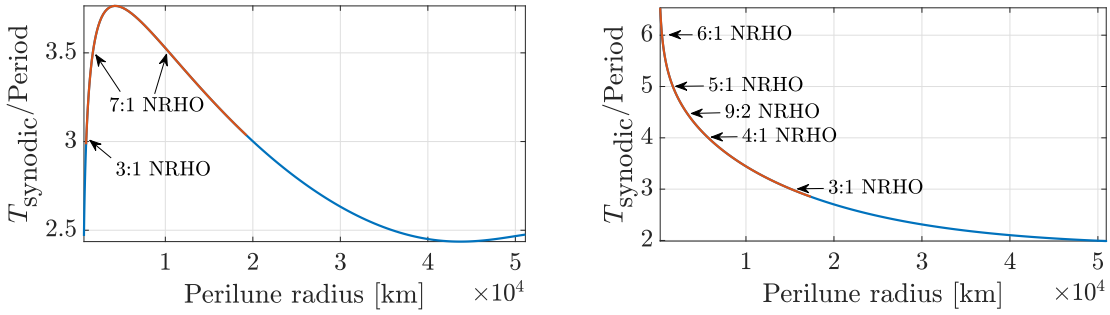

Figure 3: **Synodic resonance across the CR3BP Earth-Moon L_1 (a) and L_2 (b) halo families. Members of the NRHO subset are colored in orange.**

resonance ratio may exist along the L_1 family; for instance, there are two 7:1 resonant L_1 NRHOs in the CR3BP Earth-Moon system. On the L_2 side, the orbital period monotonically decreases along the halo family as the perilune radius decreases, as apparent in Figure 3(b). Recall that the resonance ratio is inversely proportional to the orbital period. The range over the periods in the L_2 halo family extends further than the curve on the L_1 side, thus, more single-integer ratio resonant members are present in the L_2 halo family. However, note that the resonant orbits identified in Figures 3(a) and 3(b) comprise only a sample of the resonant NRHOs. Orbits possessing more complex resonance ratios, for instance, 61:17, are also synodic resonant orbits, although less obviously useful. While there is an infinity of synodic resonant NRHOs, this investigation generally focuses on NRHOs with single-integer resonant ratios.

Corrections process

To construct a BCR4BP periodic solution from a synodic resonant CR3BP orbit, the most successful strategy employs a continuation process. An effective continuation parameter is a coefficient that scales the mass of the Sun,[11] that is, varies between zero, corresponding to the Earth-Moon CR3BP, and unity, reflecting the Earth-Moon-Sun BCR4BP. To transition between the models, a new pseudo-

potential, Γ^*, is defined

$$\Gamma^* = U^* + \frac{\epsilon\, m}{r_{\text{s-sc}}} - \frac{\epsilon\, m}{a^3}(x_{\text{s}}x + y_{\text{s}}y + z_{\text{s}}z) \tag{8}$$

such that ϵ is the coefficient to scale the mass of the Sun. Note that for $\epsilon = 0$, the updated pseudo-potential Γ^* is equivalent to the CR3BP pseudo-potential, introduced in Equation (2). Conversely, for $\epsilon = 1$, Equation (8) is equivalent to the BCR4BP pseudo-potential, in Equation (5).

The transition of the orbit between the models is achieved using one step in ϵ, i.e., one jump from zero to one, or by breaking the continuation procedure into multiple steps. The results from an example of the latter strategy appear in Figure 4. In this example, the initial orbit is the 3:1 synodic resonant NRHO in the CR3BP, that appears in light blue in Figure 4. Its orbital period is exactly

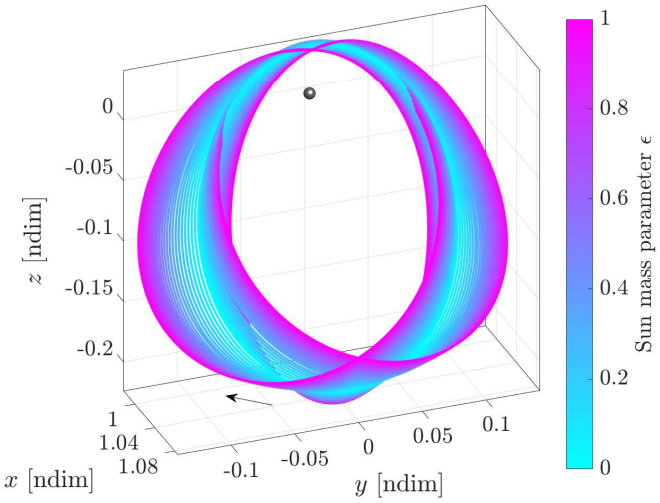

Figure 4: **Continuation orbits between the CR3BP 3:1 resonant NRHO (in light blue) and its final BCR4BP periodic counterpart (in purple).**

one third of the synodic period. Therefore, the orbital period of the BCR4BP periodic solution is a synodic period. To transition a trajectory from the CR3BP to a higher-fidelity model involves a straightforward targeting scheme. Three revolutions of the 3:1 synodic resonant NRHO in the CR3BP are stacked on top of each other to form the initial guess. (Note that more sophisticated targeting strategies that accommodate constraints and alternative goals are also available. But the simplified approach is sufficient in this example.) The solution is then discretized into patch points to facilitate the convergence process. While a single-shooter algorithm is an acceptable alternative, the BCR4BP periodic orbits typically possess longer periods and more 'loops' than their CR3BP counterparts. Thus, a parallel-shooting scheme is typically more robust for this type of scenario. At each step, represented by the evolving value of the mass parameter, ϵ, the solution is propagated and corrected for continuity between consecutive patch points and for periodicity. Once a solution for a given ϵ value is computed, it is employed as the initial guess for the next step in the continuation procedure. In the example in Figure 4, 25 equally-spaced steps between $\epsilon = 0$ and $\epsilon = 1$ are introduced, and the converged, periodic solution for each step is plotted. The solution corresponding to $\epsilon = 1$, colored in purple in Figure 4, corresponds to the Earth-Moon-Sun BCR4BP periodic

solution. Any BCR4BP periodic orbit is constructed using a synodic resonant CR3BP orbit as the initial guess in a continuation process with the Sun mass as the continuation parameter.

BCR4BP Near Rectilinear Halo Orbits

Multiple synodic resonant NRHOs that are identified in the resonance plot in Figure 3(b) are transitioned from the CR3BP to the BCR4BP. As the L_2 family evolves out of plane and approaches the Moon, the first single-integer, synodic resonant orbit encountered in the NRHO subset is the 3:1 NRHO, since the 2:1 resonant halo is not part of the NRHO subset. This 3:1 resonant NRHO is characterized by a period exactly equal to one third of the Earth-Moon synodic period, that is, approximately 9.79 days, a perilune radius of about $15,000$ km and an apolune radius of approximately $84,500$ km, as plotted in Figure 5(a). To build the initial guess for the BCR4BP periodic

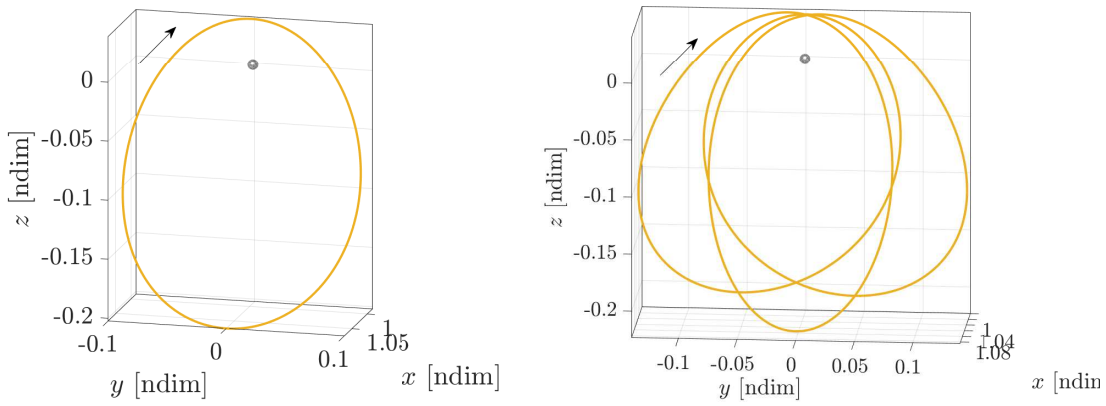

(a) (b)

Figure 5: **CR3BP 3:1 NRHO (a) and its T_{syn}-periodic BCR4BP counterpart (b).**

solution, three revolutions of this NRHO are stacked, thus forming a periodic orbit with a period precisely equal to a synodic period. This initial guess is then corrected and continued, using the methodology described previously, until the BCR4BP periodic solution, appearing in Figure 5(b), is produced. This periodic orbit has a period precisely equal to the Earth-Moon synodic period, thus, it is also labeled a 'T_{syn}-periodic' orbit in this investigation. The BCR4BP periodic orbit includes three distinct lobes, each corresponding to a revolution along the initial stack. One lobe is stretched in the $\hat{y}$ direction, the other is stretched in the $-\hat{y}$ direction, and the third lobe is centered with respect to the $\hat{y}$ axis. This stretching corresponds to the Sun perturbing acceleration. A perilune and an apolune occurs along each of the lobes. The perilune radii range between $14,300$ and $15,200$ km, while the apolunes radii are between $82,300$ and $89,400$ km.

As the perilune radius decreases, the second simple resonance ratio encountered in Figure 3(b) is the 4:1 CR3BP NRHO. This NRHO is characterized by a period precisely equal to a quarter of the Earth-Moon synodic resonance, that is, 7.34 days, and appears in Figure 6(a). The perilune radius is approximately equal to $5,600$ km and the apolune radius is about $75,335$ km. The BCR4BP T_{syn}-periodic counterpart of the CR3BP 4:1 NRHO is plotted in Figure 6(b). First, note that there are actually four lobes in Figure 6(b): at a finer scale, two distinct revolutions are apparent on each of the two obvious lobes. This 'superposition' is due to the geometry of this BCR4BP periodic orbit. Tidal effects[12] from the Sun introduce similar effects in two opposite quadrants representing the Sun

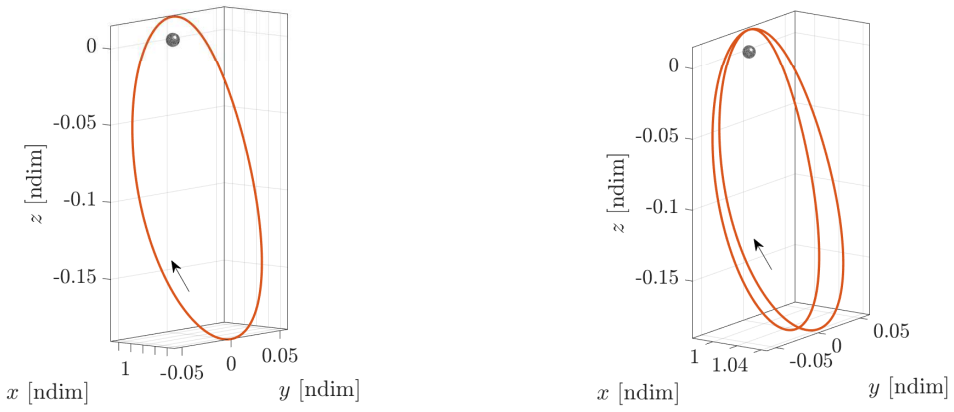

(a) (b)

Figure 6: **CR3BP 4:1 NRHO (a) and its BCR4BP T_{syn}-periodic counterpart (b).**

angle θ_S between 0° and 90°, and the quadrants between -180° and -90°. Conversely, the tidal effects are also similar for Sun angle quadrants defined between 0° and -90°, as well as between 90° and 180°. Therefore, the first and the third revolutions of the BCR4BP T_{syn}-periodic orbit are 'pulled' by the Sun gravitational acceleration in one direction; the second and the fourth revolutions are impacted by the solar acceleration in the opposite direction, as apparent in Figure 6(b). Note that the stretching of the lobes occurs in the positive and negative $\hat{x}$ directions, as opposed to the $\hat{y}$ direction in Figure 5(b). The apolune radii range between $74,800$ and $75,500$ km, while all four perilune radii are approximately equal to $5,900$ km.

The next synodic resonant orbit transitioned to the BCR4BP is the 9:2 NRHO. Note that, in contrast to the previous orbits, this solution exhibits a N:2 resonance. Nine revolutions along the 9:2 NRHO precisely correspond to two Earth-Moon synodic periods, that is, 59 days. The 9:2 synodic resonant NRHO, along with the 4:1 synodic resonant NRHO, are potential candidate baselines for a long-term facility in cislunar space due to their eclipse-avoidance properties.[6,13] The CR3BP 9:2 NRHO is characterized by a period of 6.53 days, a perilune radius of approximately $3,100$ km and an apolune radius of about $71,000$ km, as plotted in Figure 7(a). Observe that the initial guess for the transition procedure is constructed by stacking nine revolutions of the 9:2 NRHO in the CR3BP. The 2 T_{syn}-periodic solution produced in the BCR4BP appears in Figure 7(b). This periodic solution in the BCR4BP includes 9 lobes and, thus, 9 low-altitude perilunes. Strong nonlinear effects occur in the close vicinity of the primaries. Therefore, the continuation and corrections procedures from the 9:2 synodic resonant NRHO in the CR3BP to the 2 T_{syn}-periodic orbit in the BCR4BP presents many numerical challenges. Multiple approaches are possible to mitigate these difficulties, including an increase in the number of patch points along the orbit, as well as using a line search[14] strategy during the corrections procedures. Note that, despite the long period, the geometry of the periodic orbit in the CR3BP is maintained in the BCR4BP. The perilune radii range (between $3,100$ and $3,900$ km) in Figure 7(b) and the range of apolunes radii (between $69,900$ and $71,700$ km) for the 2 T_{syn}-periodic solution in the BCR4BP are also consistent with the 9:2 NRHO in the CR3BP.

The fourth and last L_2 NRHO examined in this investigation is the synodic resonant 5:1 NRHO. As the perilune radius decreases, the orbital period asymptotically decreases, as apparent in Figure 3(b). Hénon[15] demonstrated that an asymptotic evolution of a parameter along a family of solutions

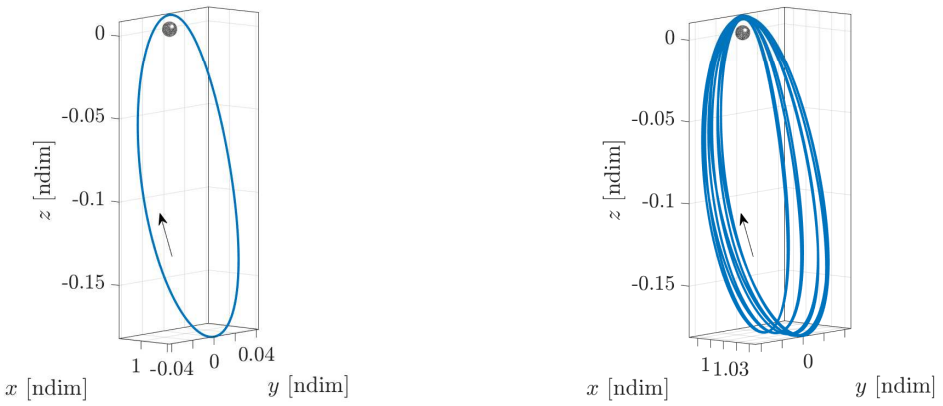

(a) (b)

Figure 7: **CR3BP** 9**:**2 **NRHO (a) and its BCR4BP** 2 T_{syn}**-periodic counterpart (b).**

signifies the end of this family. Thus, the L_2 halo family of orbits in the CR3BP presents two distinct termination locations: one is the bifurcating orbit from the planar Lyapunov family, and the other occurs at this asymptote. Note that such is not the case along the L_1 halo family in the CR3BP: the family continues further than the members plotted in Figures 2(a) and 3(a). The synodic resonant 5:1 NRHO is plotted in Figure 8(a): with a perilune radius of $1,650$ km (and an apolune radius of $66,000$ km), the orbit visibly impacts the Moon. Recall that the primaries are assumed to be point masses in the CR3BP. There is no knowledge concerning the Moon radius (equal to $1,730$ km) in the equations of the motion in Equations (1) and (4), thus, any solution impacting the Moon, periodic or not, is a valid mathematical solution. The T_{syn}-periodic orbit in the BCR4BP corresponding to the 5:1 NRHO appears in Figure 8(b). The five perilunes include radii between $1,500$ and $3,000$ km, while the radii corresponding to the five apolunes range between $64,500$ km and $68,200$ km. Therefore, not all lobes along the periodic solution in the BCR4BP encounter the lunar surface. The five lobes are distributed as follows: two front lobes are located at $x > x_{\text{m}}$, where x_{m} is the

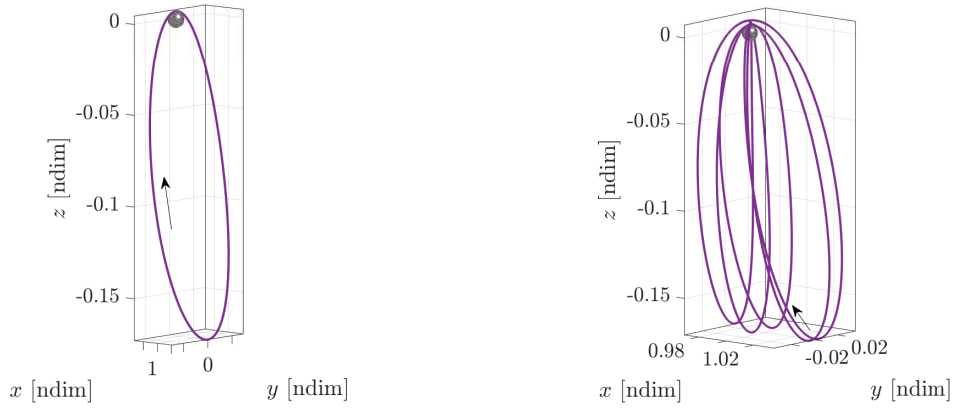

(a) (b)

Figure 8: **CR3BP** 5**:**1 **NRHO (a) and its BCR4BP** T_{syn}**-periodic counterpart (b).**

x-coordinate of the Moon, two middle lobes are located at approximately the same x coordinate as the Moon, and the last lobe is on the L_1 side of the Moon. The highest perilunes correspond to connections from a front lobe to the back lobe, similar in geometry to some members of the L_2 butterfly family. The butterfly family bifurcates from the halo family in the vicinity of the NRHO subset, thus, it is not surprising to discover flow patterns shared by the two families.[8,16]

The four previous synodic resonant NRHOs of interest in the CR3BP are plotted together in Figure 9(a). Recall that they are selected for their periods: all four orbits are single-digit synodic resonant orbits from the L_2 halo family. The four periodic orbits in Figure 9(a) are the basis for the construction of the solution in the BCR4BP via the continuation/corrections procedure, and the result appears in Figure 9(b). The N:1 synodic orbits are continued to T_{syn}-periodic orbits in the BCR4BP, and the 9:2 synodic NRHO is continued to a 2 T_{syn}-periodic orbit. The geometry and the apse distances to the Moon are maintained during the continuation procedure. The perturbing gravity from the Sun tends to stretch the NRHOs, mostly along the rotating $\hat{x}$ direction. The motion can be deceptively simple when represented in the Earth-Moon rotating frame in the CR3BP. When plotted in a Moon-centered inertial frame, the complexity of the dynamics becomes apparent. For instance, observe four revolutions along the 4:1 synodic resonant NRHO in the CR3BP, viewed in the Earth-Moon rotating frame in Figure 10(a). The state vectors along this periodic orbit are first shifted to Moon-centered states, then rotated to a Moon inertial frame, as apparent in Figure 10(b). Not surprisingly, the orbit does not repeat exactly when represented in the lunar inertial frame.

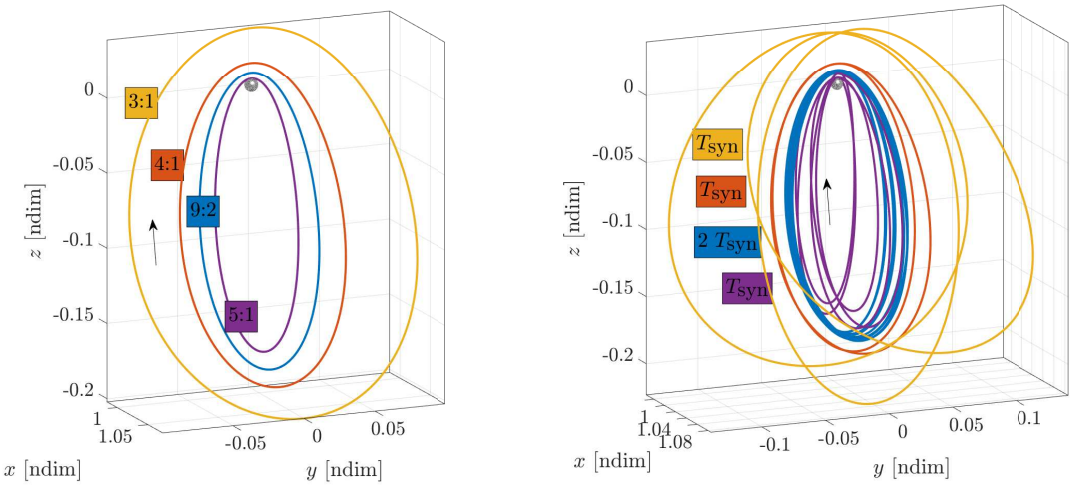

(a) (b)

Figure 9: **Four synodic resonant NRHOs as viewed in the Earth-Moon rotating frame, computed in the Earth-Moon CR3BP (a) and in the Earth-Moon-Sun BCR4BP (b).**

Energy

An examination of the energy along the N:Q synodic resonant NRHOs is also insightful. In the CR3BP, the quantity evaluated for an energy-like assessment is the Jacobi constant, defined in Equation (3). A plot of Jacobi constant values is presented in Figure 11(a). The vertical axis is the Jacobi constant value and, since the CR3BP is time-autonomous and the Jacobi constant is conserved along natural arcs, the horizontal axis demonstrates that the C value is constant against any other orbital parameter. Thus, the Jacobi constant value associated with each synodic resonant

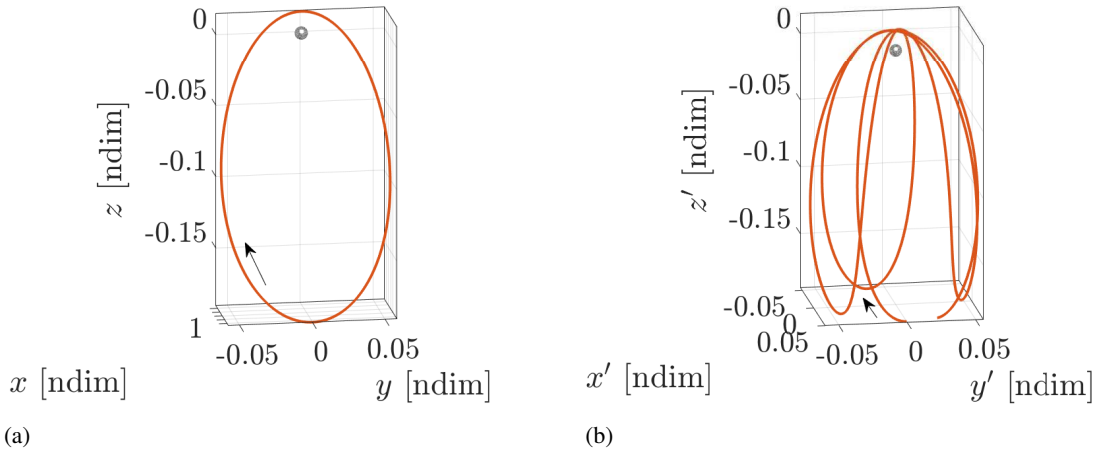

Figure 10: **CR3BP 4:1 NRHO as viewed in the Earth-Moon rotating frame (a) and in an arbitrary Moon-centered inertial frame (b).**

NRHO in the CR3BP is denoted by horizontal lines in Figure 11(a). The gray horizontal stripes represent the Jacobi constant range between each of the collinear libration points in the CR3BP: L_1, L_2 and L_3. Information about the flow is offered by the Jacobi constant values at the Lagrange points. Note that a decrease in the Jacobi constant value corresponds to an increase in energy. Thus, for Jacobi constant values above the one associated with L_1, no openings exist between the Earth and the Moon, that is, no path passes near both primaries at such an energy level. A gateway, or portal, linking regions surrounding the two primaries opens when the energy is evaluated such that $C < C_{L1}$. As the energy increases, two more gateways open: first at L_2 when $C < C_{L2}$, then at L_3 when $C < C_{L3}$.

One halo family of orbits and its subset, the NRHOs, is defined in the vicinity of the L_2 libration point. Therefore, the L_2 gateway is open, and the Jacobi constants associated with each of the synodic resonant NRHOs is below $C < C_{L2}$. The Jacobi constant associated with resonant NRHOs is linked to the perilune radius: the higher the perilune, the higher the energy along the orbit. Note that, in contrast to the resonance ratio, the evolution of the Jacobi constant across the L_2 halo family is not monotonic, as demonstrated in Figure 12. As the L_2 halo family evolves out-of-plane from the bifurcating, planar Lyapunov orbit, the energy along the family first increases and, correspondingly, the Jacobi constant decreases. A minimum value in Jacobi constant occurs as the Jacobi constant reaches the NRHO subset. Then, the energy increases as the perilune radius continues to decrease. The synodic resonant NRHOs in the CR3BP possess relatively low Jacobi constant values, and the energy is inversely proportional to the perilune altitude.

A similar analysis for the Q T_{syn}-periodic NRHOs in the BCR4BP yields further insight. Recall that the BCR4BP is time-dependent and does not possess an integral of the motion. The Hamiltonian value, defined in Equation (7), is a function of the position of the Sun as viewed in the Earth-Moon rotating frame and, thus, is a function of time. A Hamiltonian time history is plotted in Figure 11(b). The horizontal axis represents the Sun angle, i.e., θ_s, which is a linear function of the independent time variable: $\theta_s = \omega_s\, t + \theta_{s0}$. The vertical axis corresponds to the Hamiltonian value, scaled by a constant coefficient for convenience. The Hamiltonian values associated with the instantaneous libration points $E_1(\theta_S)$ through $E_3(\theta_S)$ are also indicated. Since the libration points are oscillating,

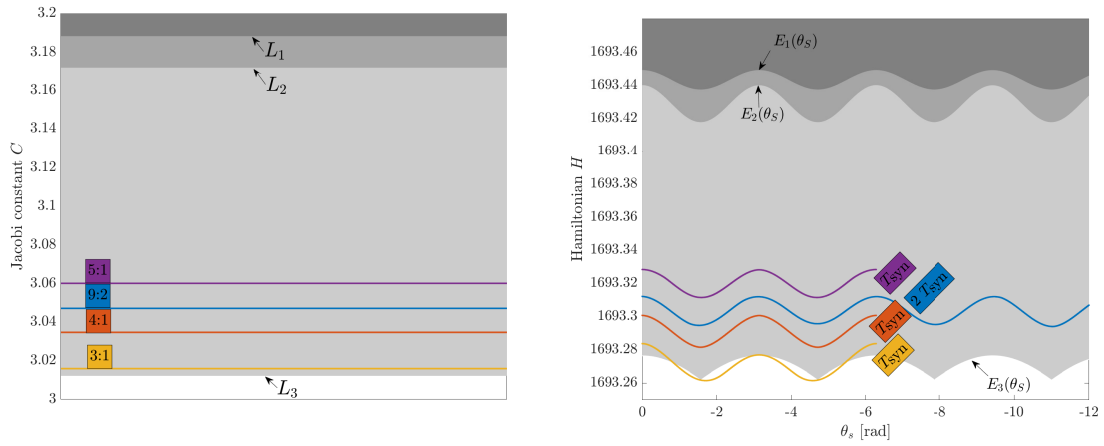

(a) (b)

Figure 11: **Energy-like quantity along the synodic resonant NRHOs: Jacobi constant in the CR3BP (a) and Hamiltonian value in the BCR4BP (b).**

their associated Hamiltonian values are also time-varying. However, the Hamiltonian values cycle over one synodic period, as do the instantaneous equilibrium points in the BCR4BP. Note that the order of the openings of the gateways in the BCR4BP is consistent with the order of opening in the CR3BP: the Zero-Velocity Curves (ZVCs) in the Earth-Moon-Sun BCR4BP are not degenerated.[17] The Hamiltonian values along one period of each of the periodic orbits in the BCR4BP are denoted by colored lines. The order of the lines is consistent with the order of the Jacobi constant values in Figure 11(a). The Hamiltonian value along T_{syn}-periodic orbit in the BCR4BP continued from the 3:1 CR3BP NRHO, i.e., the yellow line in Figure 11(b), dips below the line associated with the Hamiltonian value of $E_3(\theta)$ for certain values of θ_S. Since $E_3(\theta)$ is located on the opposite side of the Earth from the Moon, the opening or closing of $E_3(\theta)$ does not notably modify the flow in the vicinity of the orbit.

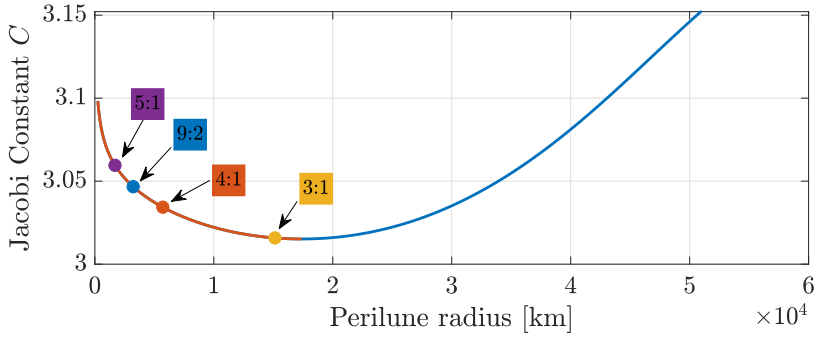

Figure 12: **Jacobi constant across the CR3BP L_2 halo family. Members of the NRHO subset are colored in orange. Synodic resonant orbits of interest are denoted by colored dots.**

Stability

The NRHO subset of the halo family is defined by its stability properties. The stability index is

a convenient metric to assess the stability of a periodic solution. The phase space in the CR3BP is six-dimensional, thus, the monodromy matrix corresponding to a periodic solution admits six eigenvalues, labeled λ_1 through λ_6. Recall from the Lyapunov theorem,[18] that eigenvalues occur in reciprocal pairs if they are real or in conjugate pairs if they are complex. Thus, each pair i of eigenvalues is combined to form three stability indices ν_i,

$$\nu_i = \frac{\lambda_i + \frac{1}{\lambda_i}}{2} \tag{9}$$

A periodic solution in the CR3BP possesses a pair of eigenvalues equal to one due to the Jacobi constant.[19,20] Therefore, a periodic orbit in the CR3BP possesses two nontrivial stability indices. If both stability indices produce an absolute value less than one, the orbit is stable in the linear sense. Otherwise, the solution is linearly unstable. The stability indices along the CR3BP L_2 halo family are plotted in Figure 13. The NRHO subset is highlighted in orange, and the previously investigated synodic resonant NRHOs are indicated by colored dots. The stability bounds, at $\nu = \pm 1$, are represented by gray lines. Two subsets of the halo family are stable in the linear sense: the subset with a perilune radius between 250 and $1,800$ km (just at the lunar surface) and an additional subset with a perilune radius between $13,300$ and $17,300$ km. The NRHO subset is comprised of the two linearly stable subsets of the halo family and the linearly unstable subset of the halo family with perilune radius between $1,800$ and $13,300$ km. Note that the stability index for this subset corresponding to the unstable mode ranges between 1 and -1.65. Thus, the instability, in the linear sense, of the members in this part of the family is therefore quite limited. Two of the synodic NRHOs constructed previously in the CR3BP are linearly stable: the 5:1 and the 3:1 synodic resonant NRHOs. The other two, the 4:1 and the 9:2 synodic resonant NRHOs are unstable, in the linear sense. However, as observed previously, the magnitude of the eigenvalue associated with the unstable mode is very low for the unstable NRHOs.

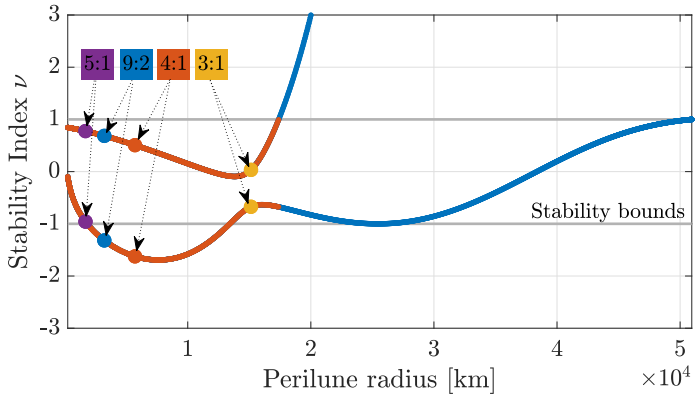

Figure 13: Stability indices across the CR3BP L_2 halo family. Members of the NRHO subset are colored in orange. Synodic resonant orbits of interest are denoted by colored dots.

Given the stability properties from the CR3BP, the stability of the periodic solutions in the BCR4BP is explored. The six eigenvalues associated with the position and velocity states for a periodic orbit in the BCR4BP occur in pairs, as the Lyapunov theorem still holds in this model. The additional eigenvalue, corresponding to the modal component of $\dot{\theta}_S = \omega_S$ is equal to unity for any trajectory, periodic or not. The partial derivatives of the differential equation $\dot{\theta}_S = \omega_S$ with respect

to the position states, the velocity states and the Sun angle, θ_S are all equal to zero, as the Sun angle is a linear function solely of the independent time variable. However, since there is no integral of the motion in the BCR4BP, the periodic solutions do not possess a pair of unit eigenvalues. Thus, three stability indices represent the variational behavior and the linear stability properties of a periodic solution in the BCR4BP.

To compare stability for the periodic solutions in the CR3BP and BCR4BP, the periods must be commensurate. Recall that a synodic resonant N:Q NRHO in the CR3BP is related to a periodic counterpart in the BCR4BP with a period equal to N times the period of the orbit in the CR3BP. However, the eigenvalues, λ_i, are functions of the number of revolutions along the periodic orbit,

$$\lambda_i(kT) = \big(\lambda_i(T)\big)^k \tag{10}$$

where T is the period and k is the number of revolutions. Thus, the eigenvalues corresponding to the synodic resonant N:Q orbits are raised to the power N to allow a meaningful comparison with the eigenvalues for the BCR4BP periodic orbits. Then, the stability index is calculated using the updated eigenvalue. For instance, the stability index along the 2 T_{syn}-periodic orbit in the BCR4BP is compared to the stability index associated with nine revolutions along the 9:2 NRHO in the CR3BP.

The stability indices for the representative synodic resonant NRHOs in the CR3BP and in the BCR4BP are listed in Table 1. The first column of the table corresponds to the three stability indices, computed for one orbital period along the orbit in the CR3BP. In the second column, the stability indices are computed for N orbital periods, where N is the first number in the N:Q resonance ratio. Note that in both the first and the second columns, one of the stability index indices is equal to unity for each of the periodic orbits. This trivial stability index corresponds to the unit pair of eigenvalues for a periodic solution in a time-autonomous system, i.e., the CR3BP. Note that there is no apparent direct relationship between the first and the second column of the table. The stability index for N periods is defined as,

$$\nu_i(kT) = \frac{\big(\lambda_i(T)\big)^k + \frac{1}{\big(\lambda_i(T)\big)^k}}{2} \tag{11}$$

and is not a simple function of the stability index associated with one period, that is, $\nu_i(kT)$. Finally, the third column of Table 1 lists the stability indices associated with a periodic orbit in the BCR4BP, computed for one orbital period. Recall that the orbital period in the BCR4BP is equal to Q lunar synodic periods, where Q is the second number in the N:Q resonance ratio. By scaling the eigenvalues by the number of revolutions in the BCR4BP, a comparison between the stability indices of the CR3BP and the BCR4BP emerges.

The stability indices for the synodic resonant 4:1 NRHO and the 9:2 NRHO are consistent between the CR3BP and the BCR4BP. Both orbits are linearly unstable, but the magnitude of the stability indices associated with the unstable modes are small. The stability indices for periodic orbits in the CR3BP for N periods are commensurate with the stability indices along the periodic solutions in the BCR4BP. For the 4:1 NRHO, the stability index associated with the stable mode is equal to -0.5267 when computed for 4 orbital periods in the CR3BP, and equal to -0.4678 in the BCR4BP. The stability index corresponding to the unstable mode is equal to 35.5053 in the CR3BP (for four revolutions of the orbit), and equal to 37.6438 along the BCR4BP periodic solution. Similarly, the stability indices for the synodic resonant 9:2 NRHO is consistent between the CR3BP and the BCR4BP. Note that the large magnitude of the stability index associated with

Table 1: **Stability indices for the sampled synodic resonant NRHOs**

Orbit	CR3BP, 1 period	CR3BP, N periods	BCR4BP, 1 period
3:1 NRHO	1 0.0334 −0.6736	1 −0.1002 0.7983	0.9694 −34.2167 0.2583
4:1 NRHO	1 0.5067 −1.6236	1 −0.5267 35.5053	0.8306 −0.4678 37.6438
9:2 NRHO	1 0.6846 −1.3183	1 0.4826 −550.1563	0.9998 0.3581 −589.6002
5:1 NRHO	1 0.7763 −0.9578	1 −0.9642 −0.1131	0.9954 −1.0240 −0.4220

unstable mode: -550 in the CR3BP and -590 in the BCR4BP, compared to 35 in the CR3BP and 38 in the BCR4BP for the synodic resonant 4:1 NRHO. This difference in order of magnitude is due to the scaling of the eigenvalues. The eigenvalues for the 9:2 NRHO are raised to the power nine, to accommodate the nine revolutions that occur in the BCR4BP, while the eigenvalues from the 4:1 NRHO are raised to the fourth power. When comparing the stability indices associated with one CR3BP orbital period, that is, the first column in Table 1, it is clear that the 4:1 and the 9:2 NRHOs possess very similar stability characteristics. As noted previously, the unit stability index is not conserved in the BCR4BP. The third stability index is associated with a stable mode with magnitude close to one: 0.9998 for the BCR4BP periodic counterpart of the 9:2 NRHO and 0.8306 for the BCR4BP periodic counterpart of the 4:1 NRHO. The stability properties of the synodic resonant 4:1 and 9:2 NRHOs are maintained when the orbits are transitioned to the BCR4BP.

Some differences in the stability characteristics between the CR3BP and the BCR4BP models are present for the 3:1 and the 5:1 NRHOs. Both synodic resonant orbits are linearly stable in the CR3BP, and linearly unstable in the BCR4BP. Note that the magnitude of the stability index associated with the unstable mode along the 5:1 BCR4BP NRHO is very close to one (-1.0240). Thus, perturbed motion in the vicinity of the 5:1 NRHO remains close to the periodic orbit for an extensive length of time, despite the linearly unstable nature of the solution, as expected for such a low stability index since the associated time constant for the unstable mode is large. The stability characteristics vary more significantly between models for the synodic resonant 3:1 NRHO. In the CR3BP, the periodic orbit is stable, in the linear sense. The solution constructed in the BCR4BP from this periodic, linearly stable initial guess is unstable. The stability index associated with the unstable mode is equal to -34.2167. This important difference in stability characteristics might suggest that the BCR4BP periodic orbit is not the true counterpart of the synodic resonant 3:1 NRHO. This possibility is still being investigated. With the exception of the 3:1 NRHO, the stability characteristics are generally consistent for periodic solutions obtained in the CR3BP and in the BCR4BP.

Eclipse-avoidance properties

Eclipse events can have considerable repercussions on a mission. Power and temperature require-

ments may not be achieved when the spacecraft is in the shadow of a celestial body. Minimal time without Earth communications can also be a mission requirement. Thus, eclipse-avoidance is often a major component in the trajectory design process.[6,21] The NRHO subset of the L_2 halo family presents multiple eclipse-avoidance properties. Recall that the NRHOs are out-of-plane orbits and almost aligned with the rotating $\hat{z}$-axis, as observed in Figure 2(b). Therefore, the time spent in the x-y plane and, thus, potentially in the shadow of one of the primaries is limited. Another eclipse-avoidance property derives from the synodic resonance characteristics of particular NRHOs. Recall the synodic period is the time between two alignments of the Sun, the Earth and the Moon. Thus, the synodic period is closely related to the eclipses. Earth shadows are avoided by phasing the spacecraft in orbit such that it is closer to apolune as the Earth shadow passes. Lunar shadows are minimized via the orbital orientation in the Sun-Moon reference frame. Lunar shadow avoidance, i.e., minimization of the time spent by the spacecraft in the shadow of the Moon, is explored for two synodic resonant NRHOs.

The Sun-Moon rotating frame is a convenient frame for exploring the impact of the lunar shadow on a given trajectory. In this rotating frame, the Sun and the Moon are fixed and, therefore, the lunar shadow is fixed as well. The synodic resonant 4:1 NRHO in the BCR4BP, as viewed in the Sun-Moon rotating frame is plotted in Figure 14. Note that, in this frame, the number of visible lobes and their distribution are related to the resonance ratio. The 4:1 NRHO includes four distinct lobes, that encompass the Moon once. Eclipses are then avoided by phasing the orbit such that the lunar shadow, indicated by the gray cone in Figure 14, traverses the lobes without intercepting the orbit. As visible in the top down view in Figure 14(b), the spacecraft orbit remains clear of the lunar shadow. Along with the 4:1 NRHO, the 9:2 NRHO is another potential candidate orbit for a long-term facility in the lunar orbit. The 9:2 NRHO in the BCR4BP as viewed in the Sun-Moon rotating frame is plotted in Figure 15. In this frame, the orbit presents nine lobes that encompass the Moon twice. The phasing of the lobes is selected such that the lunar shadow does not encounter the trajectory during any of the nine revolutions. Note that the lobes for the 9:2 NRHO are narrower than ones of the 4:1 NRHO. Thus, phasing the trajectory to avoid the lunar shadow may be more challenging for the 9:2 NRHO due to these narrower gaps. The Sun angle, θ_S, that defines the Earth-

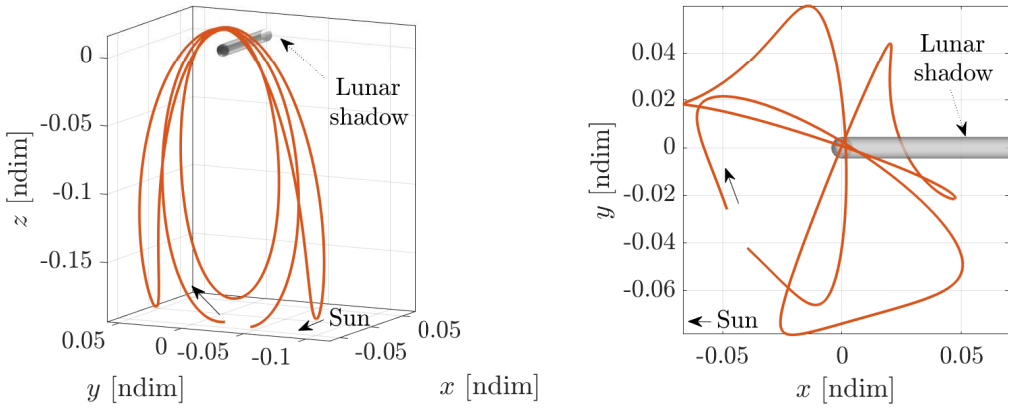

(a) (b)

Figure 14: **BCR4BP 4:1 NRHO and lunar shadow, as viewed in the Sun-Moon rotating frame centered at the Moon.**

Moon-Sun relative geometry, is the phasing parameter. By varying this parameter, the orientation of the lobes in the Sun-Moon frame is adjusted. Operationally, this variation is equivalent to shifting the injection date. Note that in the Sun-Moon rotating frame, the Earth is moving and the shadow from the Earth may encounter the trajectory if the spacecraft location in the orbit is not correlated with the Earth shadow.

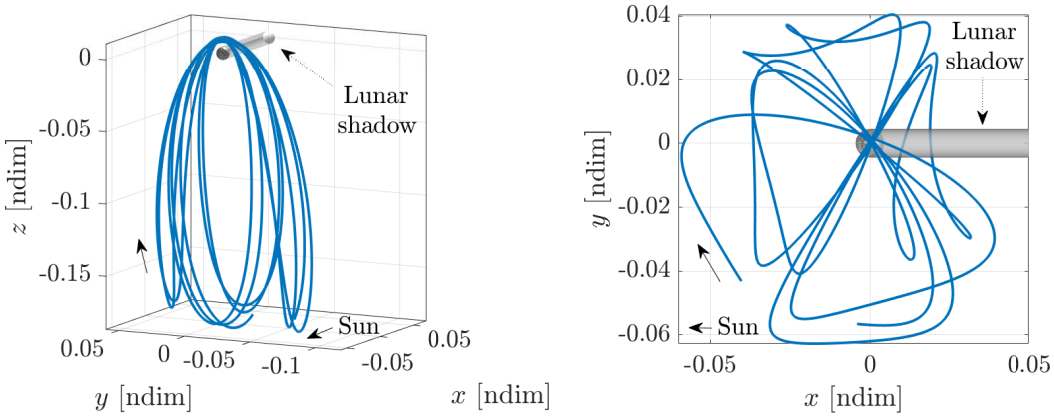

(a) (b)

Figure 15: **BCR4BP 9:2 NRHO and lunar shadow, as viewed in the Sun-Moon rotating frame centered at the Moon.**

APPLICATION: NRHO-TO-EARTH INITIAL GUESS GENERATION IN THE BCR4BP

Applications for periodic orbits in the BCR4BP include the analysis of the escape dynamics from a synodic resonant NRHO in the Earth-Moon-Sun regime.[3,13] Sample departures scenarios from the proposed Gateway facility include the disposal of discarded logistics modules to heliocentric space, and departures to other destinations in the solar system, as well as return transfers to Earth. As a simple demonstration, consider departure from the NRHO and the design of a low-cost transfer to deliver a spacecraft from an NRHO to the vicinity of the Earth.

In this scenario, a spacecraft is located in the synodic resonant 3:1 NRHO in the Earth-Moon-Sun system. This spacecraft is not crewed and contains cargo for Earth return, thus, it is assumed that minimizing the fuel consumption is privileged over minimizing the time of flight. One maneuver of 20 m/s is allowed for departure from the NRHO and return to Earth proximity. Previous investigations[13] establish that aligning the maneuver direction with the velocity directions yields the fastest departure from an NRHO. The direction and the magnitude of the maneuver are established, therefore, the only remaining parameter is the location along the orbit for departure. The synodic resonant 3:1 in the BCR4BP is plotted in Figure 16, with discretized patch points denoted by colored dots. Recall that, in the BCR4BP, each state is described by three position components, three velocity components and one epoch component, i.e, the Sun angle θ_S. The color of the dots in Figure 16 represents the Sun angle. The orbital period for the 3:1 NRHO in the BCR4BP is precisely one synodic period, thus, the Sun angle associated with the patch points range from 0° to 360°. The discretization scheme selects patch points that are equally spaced in distance along the orbit, and the distance between two consecutive patch points is approximately $4,000$ km. At each of the patch

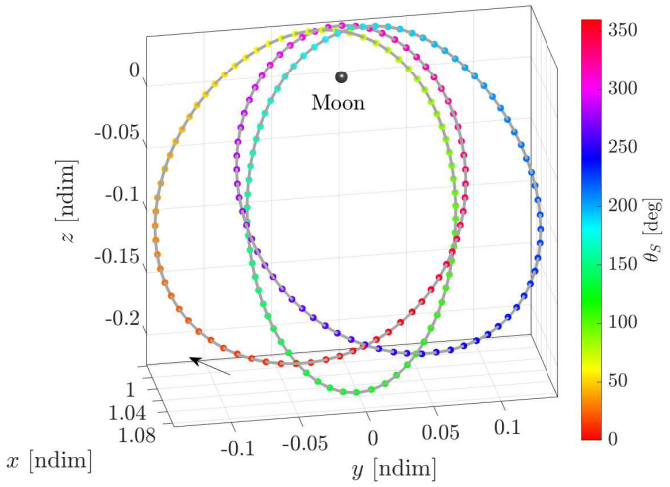

Figure 16: **Synodic resonant 3:1 NRHO in the BCR4BP**

points, a maneuver of 20 m/s is applied in the rotating velocity direction. The trajectory is then propagated for six months in the BCR4BP.

Potential transfers from the 3:1 NRHO are transfers than encounter the Earth proximity in less than the 6-month limit. The Earth proximity is defined as a sphere of radius $60,000$ km centered at the Earth. Note that this proximity definition is set for the purpose of the example, and is clearly variable for other applications. Sample transfers that are successful appear as viewed in the Earth-Moon rotating frame in Figure 17. All trajectories reflect a similar geometry: one or more loops around the Earth-Moon system, before entering the Earth vicinity, represented by a gray disk. From the color scale in Figures 16 and 17, most transfers to the Earth vicinity exist under the specified conditions when the maneuver is implemented near the apolune on one of the side lobes in Figure 16. These locations along the 3:1 NRHO are defined for a Sun angle between 200° and 250°.

As the spacecraft completes many revolutions around the Earth-Moon system, additional insight is apparent by representing the trajectory in the Sun-B_1 rotating frame. In this frame, the Sun and the Earth-Moon barycenter, i.e., B_1, are fixed, while the Earth and the Moon are assumed to be in circular orbits around B_1. Note that the motions of the primaries in this frame are consistent with the definition of the BCR4BP. The state vectors obtained using the BCR4BP equations of the motion in the Earth-Moon rotating frame from Equation (4) are rotated to the Sun-B_1 frame or, equivalently, the initial conditions can be rotated and propagated using a different set of equations of the motion for the BCR4BP defined in terms of the Sun-B_1 rotating frame.[4]

The NRHO-to-Earth transfers viewed in the Sun-B_1 rotating frame are plotted in Figure 18. In this figure, the Sun is located on the far left, the lunar orbit is represented by a light gray line, and the Earth proximity, which encompasses the Earth orbit, by a dark gray disk. When represented in this frame, the trajectories complete one distant apoapse with respect to the Earth, before re-entering the Earth-Moon system. A set of quadrants, centered at B_1, is defined to facilitate the investigation of the net perturbing acceleration due to the Sun, or tidal acceleration.[12] Note that all the trajectories plotted in Figure 18 possess a periapse with respect to the Earth located in either quadrant I or quadrant III. For trajectories with apoapses in these quadrants, the perturbing effects from the Sun tend to elongate the trajectories and decrease the periapse radius. In fact, the periapses along the

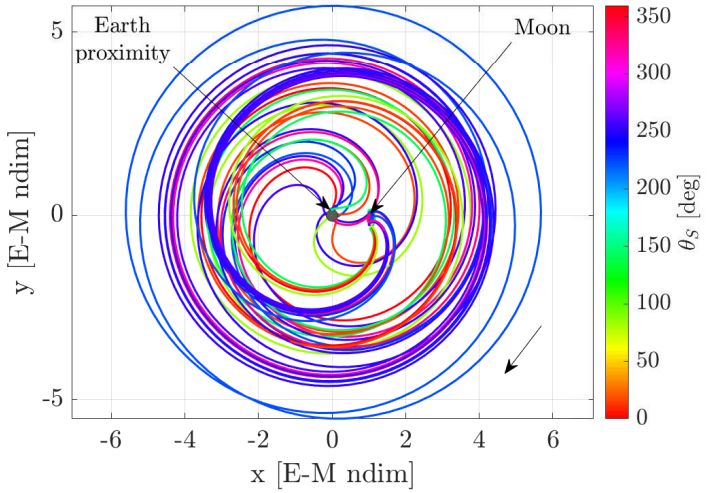

Figure 17: **Sample transfers from the 3:1 NRHO to the Earth proximity in the BCR4BP, viewed in the Earth-Moon rotating frame.**

trajectories are lowered significantly to reach the Earth proximity. Note that the trajectories in Figure 18 resemble lunar ballistic transfers,[22] but in reverse direction, as lunar ballistic transfers are defined as transfers from the Earth to the lunar vicinity. By modeling this scenario in the BCR4BP, the solar gravity is leveraged to obtain multiple low-cost initial guesses for an NRHO-to-Earth transfer.

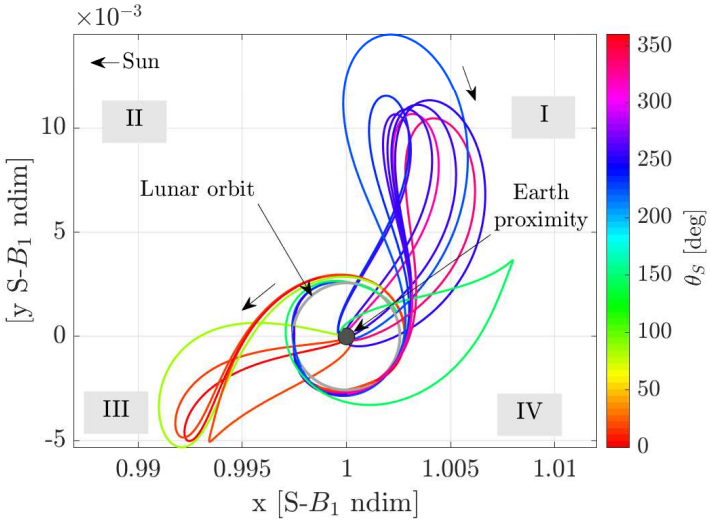

Figure 18: **Sample transfers from the 3:1 NRHO to the Earth proximity in the BCR4BP, viewed in the Sun-B_1 rotating frame.**

CONCLUDING REMARKS

Near rectilinear halo orbits are currently proposed as the baseline trajectory for a facility planned to serve as a hub for upcoming activities in the lunar region. Yet to support various pathways

throughout the region, solar gravity

REFERENCES

[1] K. Hambleton, "Deep Space Gateway to Open Opportunities for Distant Destinations," https://www.nasa.gov/feature/deep-space-gateway-to-open-opportunities-for-distant-destinations, 2017.
[2] C. Warner, "NASA's Lunar Outpost will Extend Human Presence in Deep Space," https://www.nasa.gov/feature/nasa-s-lunar-outpost-will-extend-human-presence-in-deep-space, 2018.
[3] K. K. Boudad, D. C. Davis, and K. C. Howell, "Disposal Trajectories from Near Rectilinear Halo Orbits," *AAS/AIAA Astrodynamics Specialist Conference*, Snowbird, Utah, 2018.
[4] K. K. Boudad, *Disposal Dynamics From The Vicinity Of Near Rectilinear Halo Orbits In The Earth-Moon-Sun System*. M.S. Thesis, Purdue University, West Lafayette, Indiana, 2018.
[5] M. A. Andreu, *The Quasi-Bicircular Problem*. PhD Dissertation, Universitat de Barcelona, 1998.
[6] E. M. Zimovan, K. C. Howell, and D. C. Davis, "Near Rectilinear Halo Orbits and their Application in Cis-Lunar Space," *Advances in the Astronautical Sciences*, 2017.
[7] K. C. Howell, "Families of Orbits in the Vicinity of the Collinear Libration Points," *The Journal of the Astronautical Sciences*, 2001.
[8] D. J. Grebow, *Generating Periodic Orbits in the Circular Restricted Three-Body Problem with Applications to Lunar South Pole Coverage*. M.S. Thesis, Purdue University, West Lafayette, Indiana, 2006.
[9] A. E. Roy, *Orbital Motion*. Routledge, 2004.
[10] R. A. Broucke, "Stability of Periodic Orbits in the Elliptic, Restricted Three-Body Problem," *AIAA Journal*, 1969.
[11] G. Gómez, J. Llibre, R. Martínez, and C. Simó, *Dynamics and Mission Design Near Libration Points*. World Scientific Publishing Company, 2001.
[12] D. C. Davis, *Multi-Body Trajectory Design Strategies Based on Periapsis Poincaré Maps*. PhD Dissertation, Purdue University, West Lafayette, Indiana, 2011.
[13] D. C. Davis, K. K. Boudad, S. M. Phillips, and K. C. Howell, "Disposal, Deployment, and Debris in Near Rectilinear Halo Orbits," *AAS/AIAA Astrodynamics Specialist Conference*, Ka'anapali, Maui, Hawaii, 2019.
[14] M. J. Box, D. Davies, and W. H. Swann, *Non-linear Optimization Techniques*. Oliver and Boyd for Imperial Chemical Industries, 1969.
[15] M. Hénon, *Generating Families in the Restricted Three-Body Problem*. Springer, 1997.
[16] E. M. Zimovan-Spreen and K. C. Howell, "Dynamical Structures Nearby NRHOs with Applications in Cislunar Space," *AAS/AIAA Astrodynamics Specialist Conference*, Portland, Maine, 2019.
[17] Su-Shu Huang, "Very Restricted Four Body Problem," NASA Technical Note, 1981.
[18] V. A. Yakubovich and V. M. Starzhinskii, *Linear Differential Equations with Periodic Coeffcients*, Vol. 1. New York: John Wiley and Sons, 1975.
[19] V. Szebehely, *Theory of Orbits: The Restricted Problem of Three Bodies*. Academic Press, 1968.
[20] K. R. Meyer and D. C. Offin, *Introduction to Hamiltonian Dynamical Systems and the N-Body Problem*, Vol. 90. Springer, 2017.
[21] B. P. McCarthy and K. C. Howell, "Trajectory Design Using Quasi-Periodic Orbits in the Multi-Body Problem," *29th AAS/AIAA Space Flight Mechanics Meeting*, Ka'anapali, Maui, Hawaii, 2019.
[22] J. S. Parker and R. L. Anderson, *Low-Energy Lunar Trajectory Design*. Wiley, 2014.